Energy Materials

Supplementary Material

Enhancing the long-term cycling stability of Ni-rich cathodes via regulating the length/width ratio of primary particle

Duzhao Han[1], Jilu Zhang[1], Mingyu Yang[1], Keyu Xie[2], Jiali Peng[3], Oleksandr Dolotko[3], Cheng Huang[4], Yuping Wu[5], Le Shao[6], Weibo Hua[1,*], Wei Tang[1,*]

[1]School of Chemical Engineering and Technology, Xi'an Jiaotong University, Xi'an 710049, Shaanxi, China.

[2]State Key Laboratory of Solidification Processing, School of Materials Science and Engineering, Northwestern Polytechnical University, Xi'an 710072, Shaanxi, China.

[3]Institute for Applied Materials (IAM), Karlsruhe Institute of Technology (KIT), Eggenstein-Leopoldshafen 76344, Germany.

[4]Guangdong Jiana Energy Technology Co., Ltd., Guangzhou 511449, Guangdong, China.

[5]School of Energy and Environment, Southeast University, Nanjing 210096, Jiangsu, China.

[6]Shaanxi Coal Chemical Industry Technology Research Institute Co., Ltd., Xi'an 710049, Shaanxi, China.

***Correspondence to:** Prof. Wei Tang, School of Chemical Engineering and Technology, Xi'an Jiaotong University, No. 28, West Xianning Road, Xi'an 710049, China. E-mail: tangw2018@xjtu.edu.cn; Prof. Weibo Hua, School of Chemical Engineering and Technology, Xi'an Jiaotong University, No. 28, West Xianning Road, Xi'an 710049, China. E-mail: weibo.hua@xjtu.edu.cn

Supplementary Table 1. Chemical compositions of Ni, Co and Mn for the NCM cathode powders obtained from the ICP-AES.

Samples	Chemical composition (at. %)		
	Ni	Co	Mn
HR-NCM	80.43	9.69	9.88
LR-NCM	81.01	9.55	9.84

Supplementary Table 2. Lattice parameters of HR-NCM derived from the Rietveld refinement against the sXRD patterns.

HR-NCM ($Li[Ni_{0.8}Co_{0.1}Mn_{0.1}]O_2$)					
Atom	**Site**	**x**	**y**	**z**	**Occ.**
Li1	3a	0	0	0	0.9869
Ni1	3b	0	0	0.5	0.7869
Co1	3b	0	0	0.5	0.0999
Mn1	3b	0	0	0.5	0.0999
O1	3c	0	0	0.2412	1
Li2	3b	0	0	0.5	0.0131
Ni2	3a	0	0	0	0.0131

$a = b = 2.8727(4)$ Å, $c = 14.1930(5)$ Å, Volume = 101.4372 Å^3

$\alpha = \beta = 90.0$, $\gamma = 120.0$

$R_p = 8.12\%$, $R_{wp} = 6.05\%$, $Chi^2 = 1.34$

Supplementary Table 3. Lattice parameters of LR-NCM derived from the Rietveld refinement against the sXRD patterns.

LR-NCM ($Li[Ni_{0.8}Co_{0.1}Mn_{0.1}]O_2$)					
Atom	**Site**	**x**	**y**	**z**	**Occ.**
Li1	3a	0	0	0	0.9865
Ni1	3b	0	0	0.5	0.7659
Co1	3b	0	0	0.5	0.0999
Mn1	3b	0	0	0.5	0.0999
O1	3c	0	0	0.2412	1
Li2	3b	0	0	0.5	0.0134
Ni2	3a	0	0	0	0.0134

$a = b = 2.8713(1)$ Å, $c = 14.2017(1)$ Å, Volume = 101.3988 Å^3

$\alpha = \beta = 90.0$, $\gamma = 120.0$

$R_p = 8.65\%$, $R_{wp} = 5.64\%$, $Chi^2 = 0.84$

Supplementary Table 4. Lattice parameters of cathode materials before and after cycles derived from the Rietveld refinement against the XRD patterns.

Samples	**Lattice parameters**		
	***a* (Å)**	***c* (Å)**	**Volume (Å^3)**
HR-NCM (before cycle)	2.8727(4)	14.1930(5)	101.4372
HR-NCM (after cycles)	2.8732(1)	14.2025(6)	101.5439
LR-NCM (before cycle)	2.8713(1)	14.2017(1)	101.3988
LR-NCM (after cycles)	2.8839(9)	14.3132(9)	103.0900

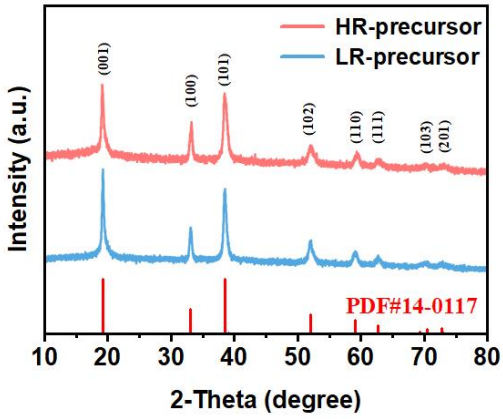

Supplementary Figure 1. XRD patterns of the hydroxide precursors synthesized under different pH conditions.

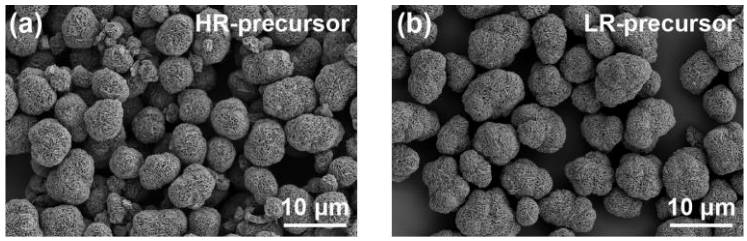

Supplementary Figure 2. The low magnification SEM images of (a) HR-precursor and (b) LR-precursor.

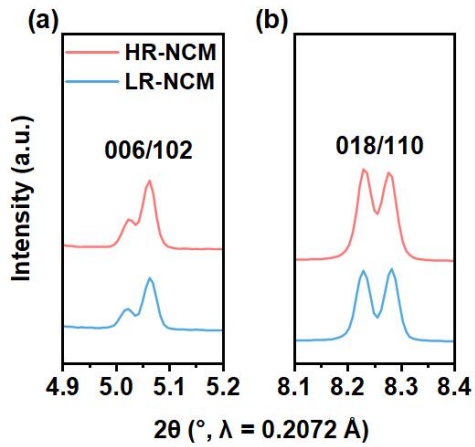

Supplementary Figure 3. Enlarged XRD patterns for (a) 006/102 and (b) 018/110 reflections of Ni-rich cathode materials.

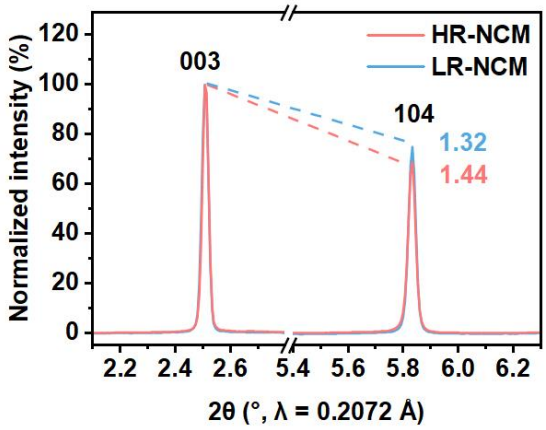

Supplementary Figure 4. The magnified XRD patterns to highlight the intensity ratio of 003/104 reflections.

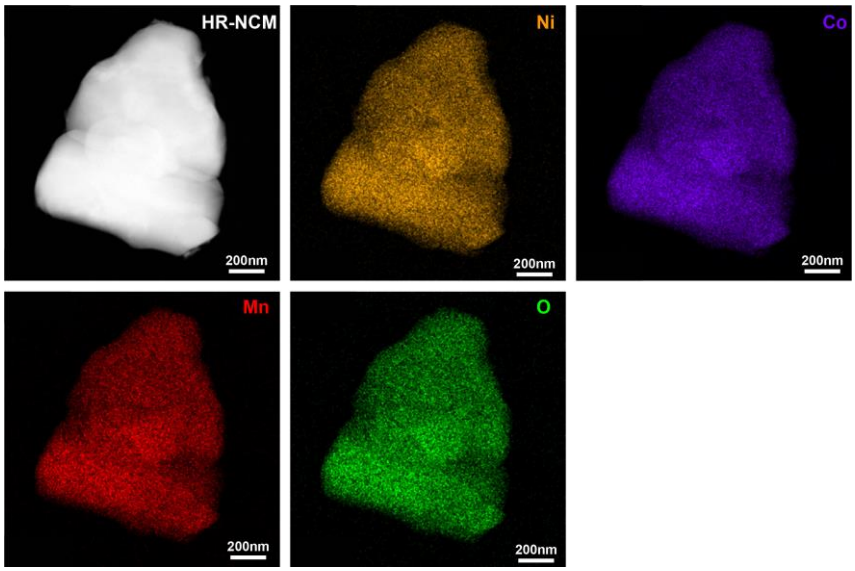

Supplementary Figure 5. TEM-EDS element mapping of Ni, Co, Mn, O in HR-NCM material.

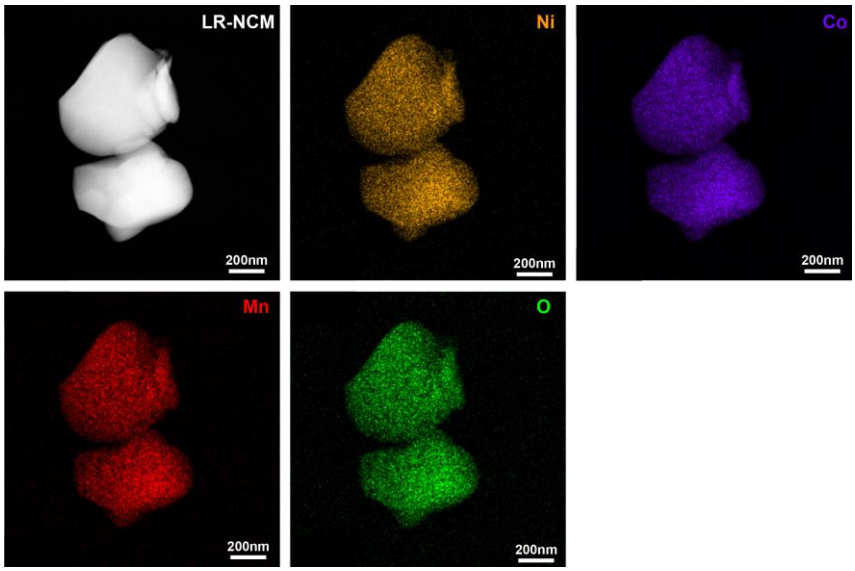

Supplementary Figure 6. TEM-EDS element mapping of Ni, Co, Mn, O in LR-NCM material.

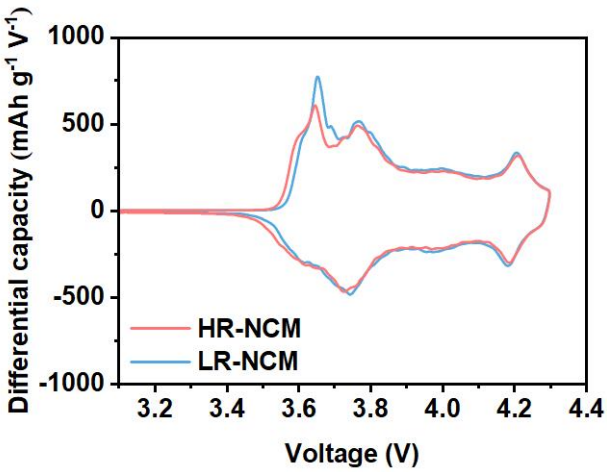

Supplementary Figure 7. dQ dV^{-1} curves of the HR-NCM and LR-NCM cathodes during the first cycle between 2.7 and 4.3 V.

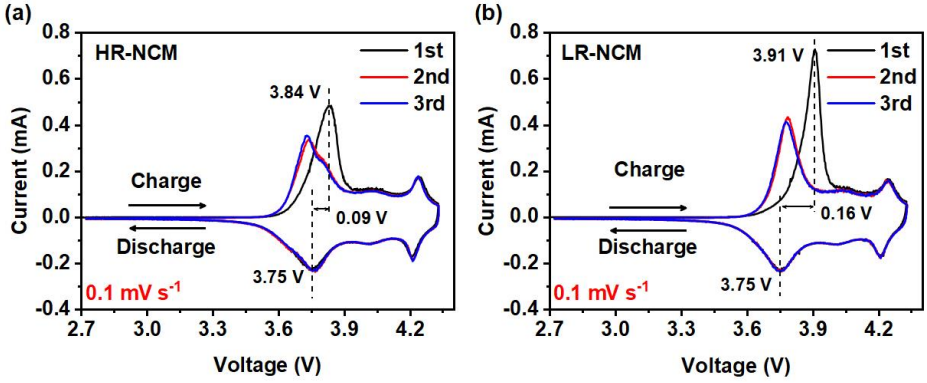

Supplementary Figure 8. CV curves of (a) HR-NCM and (b) LR-NCM cathodes with different cycles in the voltage range of 2.7-4.3 V at a scanning rate of 0.1 mV s^{-1}.

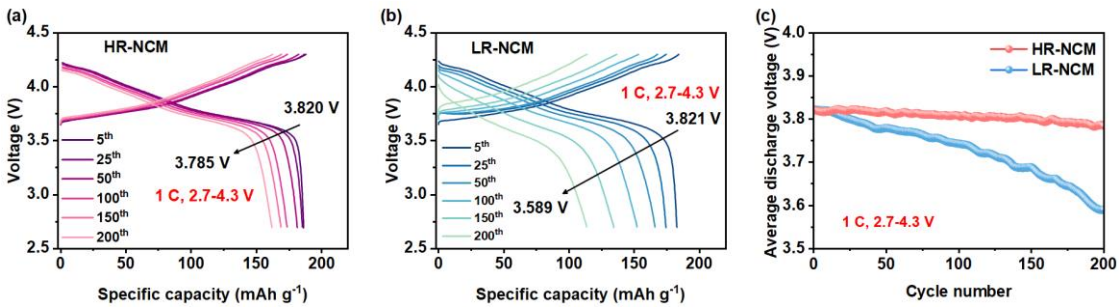

Supplementary Figure 9. Charge-discharge curves of (a) HR-NCM and (b) LR-NCM cathodes at certain cycles. (c) Corresponding voltage decay for HR-NCM and LR-NCM cathodes upon 200 cycles between 2.7 and 4.3 V.

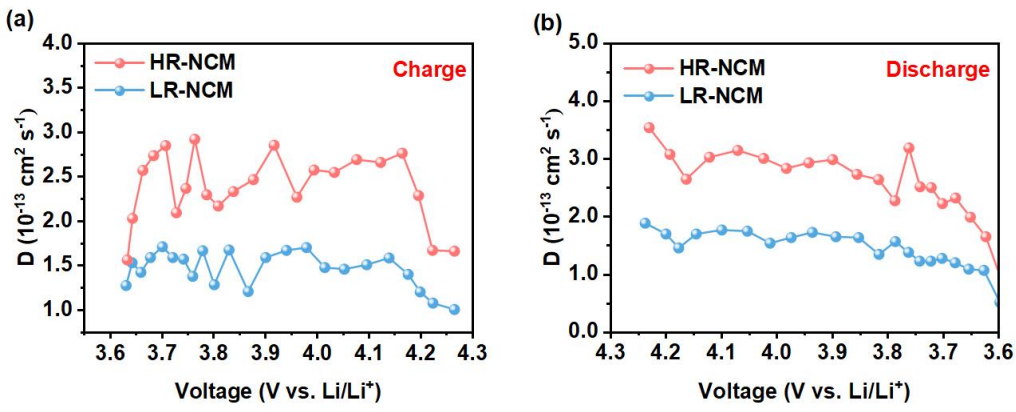

Supplementary Figure 10. Calculated apparent Li^+ diffusion coefficient obtained from GITT for HR-NCM and LR-NCM: (a) charge process and (b) discharge process.

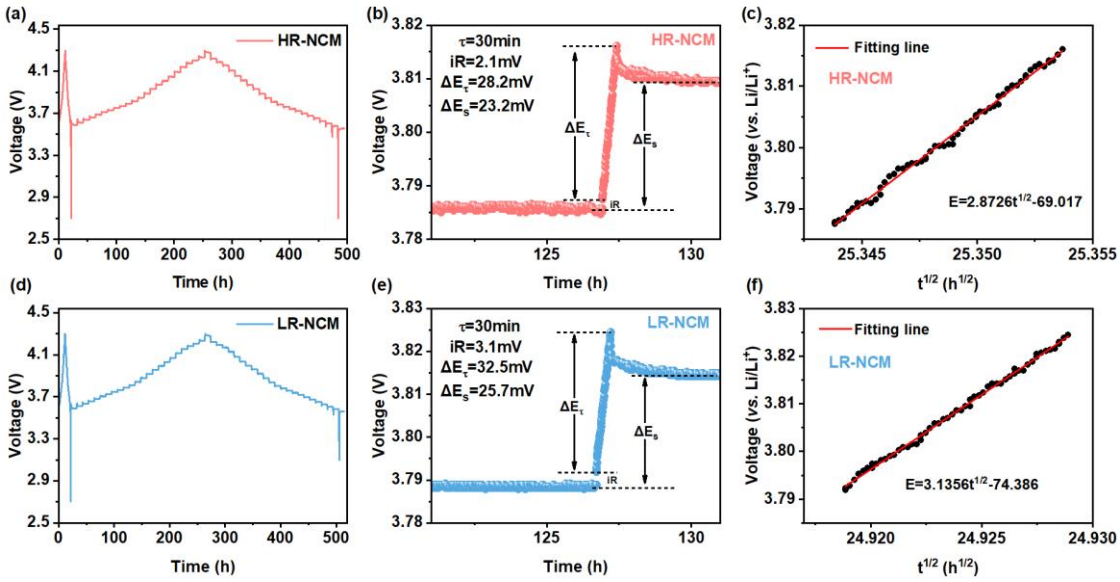

Supplementary Figure 11. GITT tests: Transient voltage-time curves, applied current pulse *vs.* voltage for a single titration about 3.8 V and corresponding variation of the potential for titration plotted against $t^{1/2}$ to show a linear fit for (a, b, c) HR-NCM and (d, e, f) LR-NCM cathodes.

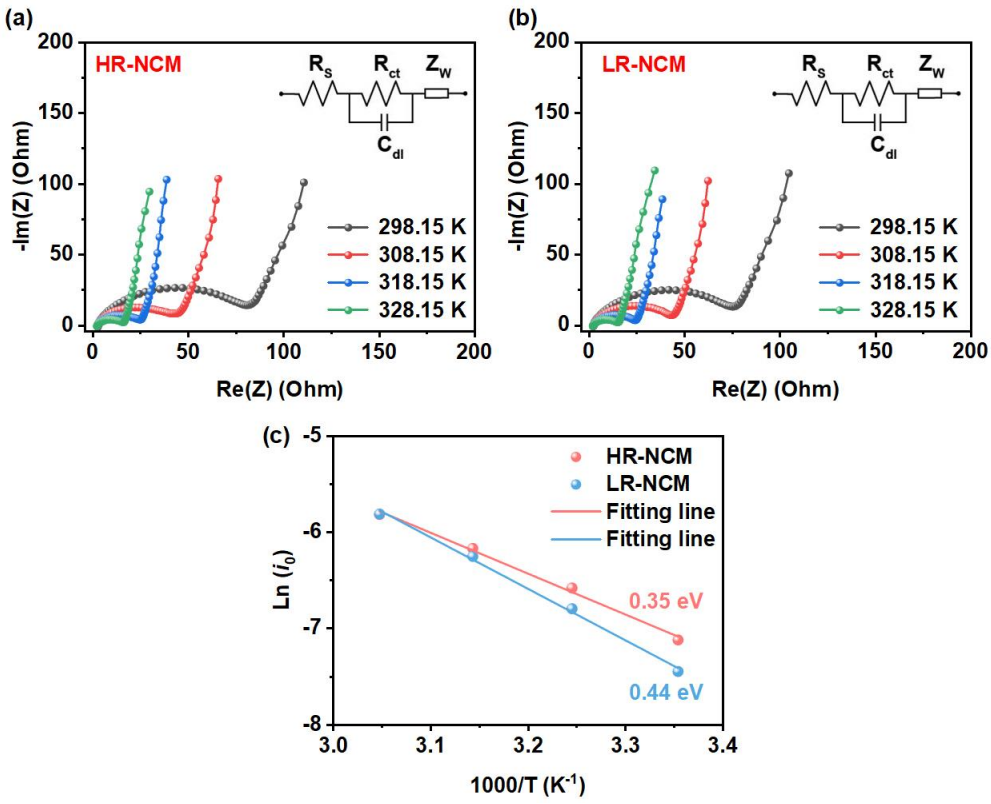

Supplementary Figure 12. EIS spectra tested under different temperatures of (a) HR-NCM and (b) LR-NCM cathodes. (c) Arrhenius plots of ln i_0 versus 1000/T for the

cathodes with the linear fitting results to calculate the apparent activation energy (E_a) of the interface reactions.

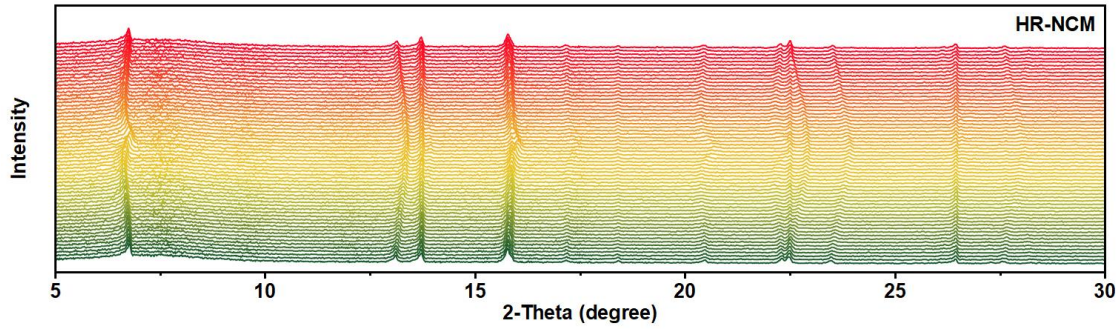

Supplementary Figure 13. Stacked profiles of the *in situ* XRD patterns of the HR-NCM cathode during the initial charge/discharge process.

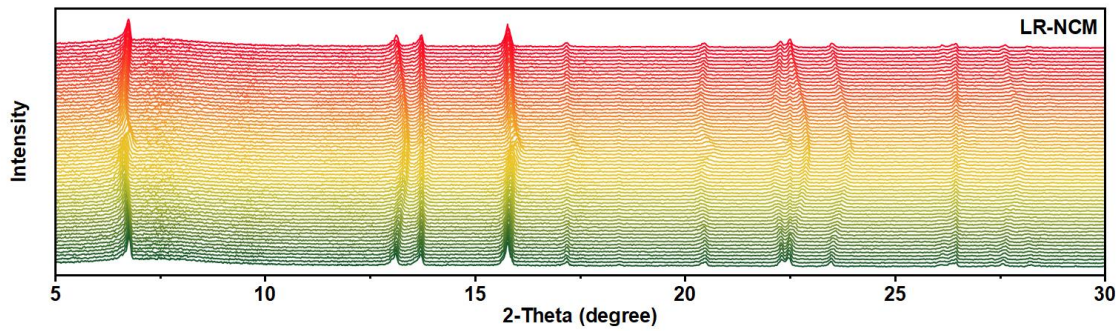

Supplementary Figure 14. Stacked profiles of the *in situ* XRD patterns of the LR-NCM cathode during the initial charge/discharge process.

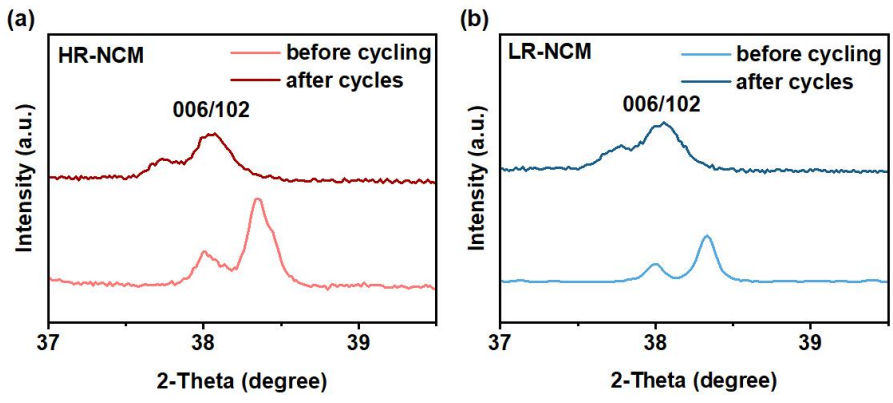

Supplementary Figure 15. Magnified XRD patterns of 006/102 splitting reflections before and after 100 cycles of (a) HR-NCM and (b) LR-NCM.

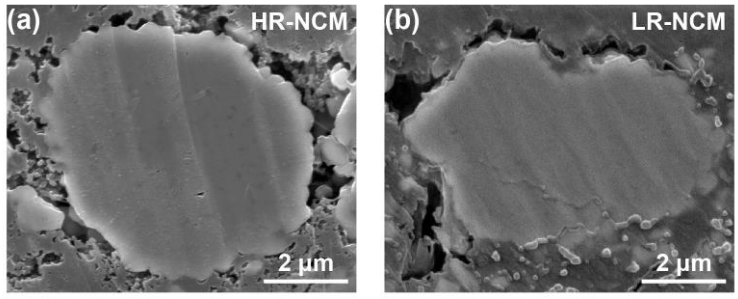

Supplementary Figure 16. The cross-sectional SEM images of uncycled (a) HR-NCM and (b) LR-NCM cathodes.

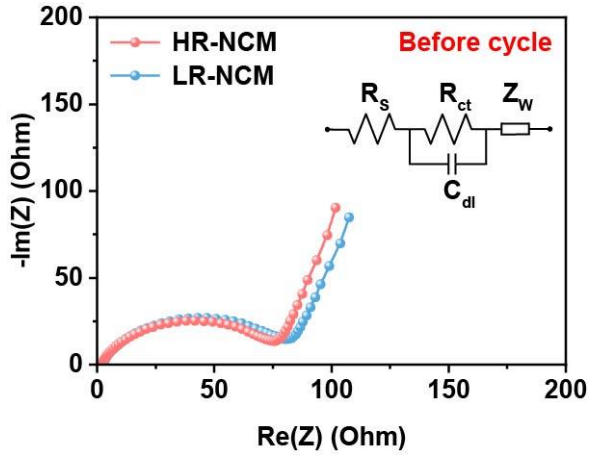

Supplementary Figure 17. EIS curves measured before cycling of HR-NCM and LR-NCM electrodes.

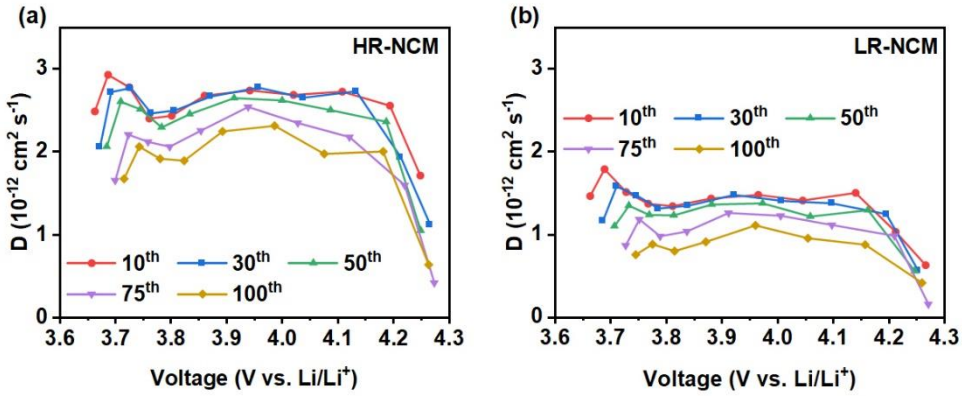

Supplementary Figure 18. The apparent ion diffusion coefficient during charging process at various cycles of (a) HR-NCM and (b) LR-NCM cathodes.